

1 Sea ice melt drives vertical pCO₂ variability modulating 2 air-sea gas exchange

3
4 Henry C. Henson^{1,2}, Dorte H. Søgaard^{2,3,7}, Bjarne Jensen⁶, Kunuk Lennert⁴, Tim
5 Papakyriakou⁵, Mikael K. Sejr^{1,2}, Jakob Sievers⁶, Søren Rysgaard^{2,7}, and Lise Lotte
6 Sørensen^{2,6}

7
8 ¹Department of Ecoscience, Aarhus University, Aarhus, 8000, Denmark

9 ²Arctic Research Center, Aarhus University, Aarhus, 8000, Denmark

10 ³Greenland Climate Research Cluster, Greenland Institute of Natural Resources, Nuuk, 3900, Greenland

11 ⁴UiT, The Arctic University of Norway, Tromsø, 9037, Norway

12 ⁵Centre for Earth Observation Science, University of Manitoba, Winnipeg, MB, R3T 2N2, Canada

13 ⁶Department of Environmental science, Aarhus University, Roskilde, 4000, Denmark

14 ⁷Department of Biology, Center for Ice-free Arctic Research, Aarhus University, Aarhus, 8000, Denmark

15
16 Corresponding author: Henry C. Henson (hch@ecos.au.dk)

17 18 19 20 21 22 **Key Points:**

- 23 • Spring melting of sea ice and snow introduces distinct heterogeneity in surface water
24 conditions within coastal Arctic oceans.
 - 25 • Standard bulk parameterizations for air-sea CO₂ flux calculations, based on subsurface
26 pCO₂ measurements, may misrepresent flux direction and magnitude during melt periods.
 - 27 • Vertical near-surface temperature and CO₂ gradients must be considered to improve flux
28 estimates in stratified Arctic fjords.
- 29

30 Abstract

31 Strong spatial and temporal gradients in salinity, temperature, and carbonate chemistry in Arctic
32 coastal surface waters complicate the estimation of air-sea carbon dioxide (CO₂) exchange,
33 particularly during sea ice breakup. This study evaluates the applicability of the widely used bulk
34 flux model under such conditions. The bulk approach assumes homogeneous surface conditions
35 and ~~linear no~~ vertical pCO₂ gradients in the bulk seawater. However, our observations in a
36 stratified Arctic fjord reveal pronounced vertical variability in pCO₂ within the upper water
37 column, including non-linear gradients near the air-sea interface. Micrometeorological flux
38 estimates suggested variability in the direction of gas transfer, measurements captured episodic
39 upward CO₂ fluxes even when waters at 1 m depth and below were CO₂-undersaturated. We
40 hypothesize that transient, high-pCO₂ layers at ~0.1 m depth within the upper decimeters
41 intermittently decouple the atmospheric exchange from subsurface waters, and have the potential
42 to reversing reverse the expected flux direction. These findings highlight the importance of
43 resolving near-surface variability during the transition from ice-covered to open water
44 conditions. We recommend incorporating micrometeorological techniques and high-resolution
45 vertical profiling in Arctic fjords to improve flux estimates of CO₂ in this rapidly changing
46 region.

47

48 Plain Language Summary

49 Sea ice melt adds less-saline water to the surface ocean. This creates vertical gradients in
50 salinity, temperature, and partial pressures of carbon dioxide (pCO₂). The concentration
51 difference of pCO₂ across the air-ocean boundary is used to estimate gas transfer. Thus, the
52 depth that we measure will impact our estimates. Directly measuring gas transfer showed both
53 CO₂ uptake and release from the ocean during sea ice breakup. This means ocean layering during
54 ice melt may briefly reverse the direction of CO₂ transfer.

55

56 1 Introduction

57 High latitude coastal oceans are strong sinks for atmospheric carbon dioxide (CO₂), absorbing
58 more CO₂ per unit area than lower latitude regions (Dai et al., 2022; Roobaert et al., 2019). This
59 strong uptake results from both the high solubility of gases in cold water and the intense
60 biological activity typical of these regions. However, climate change is rapidly transforming this
61 carbon sink. The Arctic is warming more than twice as fast as the global average, and sea ice
62 extent has been shrinking by over 13% per decade (Perovich et al., 2020). The loss of sea ice
63 increases CO₂ uptake by exposing larger areas of open water for longer periods, which can
64 further stimulate biological productivity (Arrigo and van Dijken, 2015; Bates and Mathis, 2009;
65 Perovich et al., 2020). However, at the same time, melting sea ice freshens the surface layer and
66 strengthens stratification, limiting vertical mixing with deeper water. Freshwater from melting
67 sea ice and terrestrial run-off creates pronounced gradients in physical properties such as salinity
68 and temperature, as well as chemical properties like dissolved inorganic carbon (DIC) and total
69 alkalinity (TA) (e.g. Henson et al., 2025). As a result, the partial pressure of CO₂ (pCO₂) can

70 vary markedly with depth under melt conditions (Miller et al., 2019).

71
72 This vertical variability in pCO_2 poses a challenge for air-sea CO_2 flux estimation. The transfer
73 of gases between the atmosphere and ocean depends on the difference in concentration between
74 the two as well as the efficiency of the transfer process. Therefore, the bulk flux of CO_2 across
75 the air-sea interface is commonly described as the product of the gas transfer velocity, k ($m\ s^{-1}$),
76 CO_2 solubility s ($mol\ kg^{-1}\ atm^{-1}$), and the partial pressure gradient (μatm) across the air-sea
77 interface (Wanninkhof et al., 2009):

$$78 \quad F = ks(pCO_{2_{sea}} - pCO_{2_{air}}) \quad (1)$$

79
80
81 While widely applied, this formulation simplifies a complex process influenced by surfactants on
82 the water surface, bubble-mediated gas exchange, and turbulence (Wanninkhof et al., 2009).
83 Furthermore, surface water heterogeneity, driven by sea ice melt and freshwater runoff from
84 land, complicate the physical and chemical processes governing air-sea CO_2 exchange. As a
85 result, simplified parameterizations commonly used in global carbon flux estimates may be
86 inadequate in these settings.

87
88 In many-most studies, pCO_2 is measured several meters below the surface, assuming vertical
89 homogeneity under well-mixed condition (Jørgensen et al., 2020). However, in stratified waters,
90 where temperature, salinity, and pH can vary with depth, this assumption may lead to substantial
91 errors in flux estimates (Ahmed et al., 2020; Dong et al., 2021; Miller et al., 2019; Watts et al.,
92 2022). Although Arctic surface waters are often undersaturated with respect to atmospheric CO_2
93 levels and act as CO_2 sinks (e.g., Burgers et al., 2017; Dai et al., 2022; Henson et al., 2024;
94 Laruelle et al., 2014; Roobaert et al., 2019), such assessments typically rely on sparse data
95 collected from 0.5-5 m depth during limited periods. Dong et al. (2021) illustrate that high
96 latitude fluxes of CO_2 calculated using from the bulk method (based on measurements sampled at
97 6 m depth) differ significantly from those measured using direct eddy covariance in sea ice melt
98 regions.

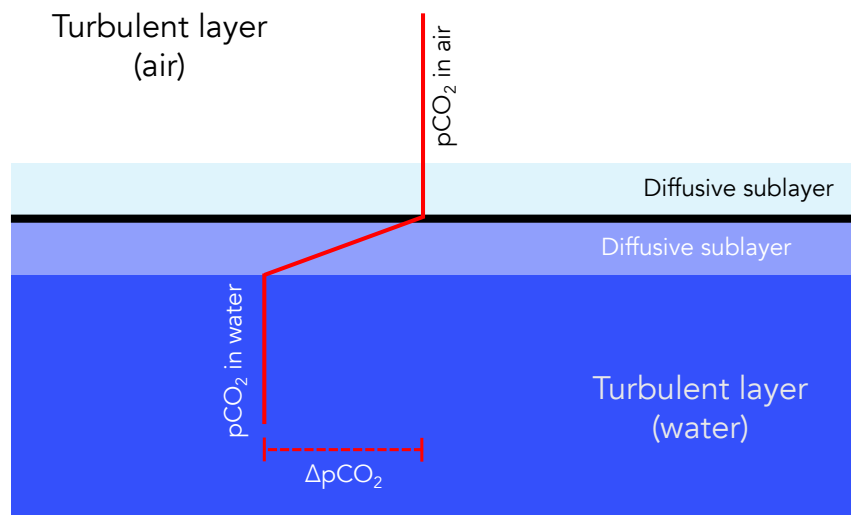
99
100 Gas transfer velocity (k) is often parameterized as a function of wind speed. However, the true
101 driver is mixing in the surface waters, which governs k . Fick's first law of diffusion, which
102 underlies Equation (1), assumes a linear concentration gradient within the diffusive sublayer
103 (Fig. 1) and steady-state conditions (Garbe et al., 2014). Jørgensen et al. (2020) argued that, due
104 to seawater's high buffer capacity, chemical gradients do not significantly affect CO_2
105 equilibration, supporting the use of measurements at 3-4 m depth. However, this conclusion
106 relies on the assumption of horizontal and vertical homogeneity and neglects the effects of
107 shallow surface stratification, particularly when alkalinity dilution is involved.

109 In Arctic spring, the upper ocean is often strongly stratified due to freshwater input from glacier
110 melt, snowmelt, river runoff, and sea ice meltwater (Ahmed et al., 2020; Granskog et al., 2011;
111 Meire et al., 2017; Miller et al., 2019). These inputs can extend vertical CO_2 gradients beyond
112 the diffusive sublayer, complicating flux estimates during ice break-up and early open-water
113 periods. Several studies have demonstrated strong vertical heterogeneity in pCO_2 in Arctic
114 coastal waters, with implications for air-sea flux calculations (Ahmed et al., 2020; Dong et al.,
115 2021; Miller et al., 2019).

116 Surface freshening from ice melt and runoff strongly influences carbonate chemistry in Arctic
117 coastal waters, which can either suppress or enhance oceanic CO_2 uptake. For example, Burgers
118 et al. (2017) reported large horizontal variability in surface pCO_2 (144–364 μatm) linked to
119 riverine input in the Eastern Canadian Arctic. Similarly, Sejr et al. (2011) observed strong
120 surface pCO_2 gradients associated with salinity and temperature in Young Sound, and later
121 documented a long-term decline in surface salinity (Sejr et al., 2017). Freshwater-induced
122 stratification has also been shown to create vertical gradients in pCO_2 and pH with important
123 implications for flux calculations (Miller et al., 2019). Finally, Bates et al. (2014) demonstrated
124 that sea ice meltwater and melt ponds exhibit extreme variability in pCO_2 (<10 to >1500 μatm)
125 and pH (6.1 to >10.8), highlighting the complex chemical landscape of ice-influenced waters.
126 Together, these studies underscore the high spatial and temporal variability of carbonate
127 chemistry in freshened waters across the Arctic.

128 To project future CO_2 uptake or outgassing in the Arctic, we must better understand the physical
129 and chemical drivers of near-surface carbonate variability. In this study, we investigate the
130 vertical and temporal variations in pCO_2 in a stratified Arctic fjord during sea ice breakup. By
131 combining ~~micrometeorological flux measurements with~~ water-column pCO_2 profiles with
132 micrometeorological flux measurements across the transition from ice-covered to open water, we
133 evaluate the performance-applicability of the bulk flux model under Arctic seasonal transitions.

134



135

136 **Figure 1.** Schematic illustrating the interface between the air and the water in conjunction with
137 pCO₂ concentration gradients. In equation 1, the concentration gradient is assumed to occur in the
138 diffusive layer between the air and water, and the concentrations are assumed to be vertically
139 constant in the turbulent layers. *(Adapted from Liss and Slater, 1974; Wanninkhof et al., 2009)*

141 2. Study Site and Measurement Methods

143 2.1 Study Site

144 This study was conducted in Young Sound, a high Arctic fjord system located near the Daneborg
145 Research Station in Northeast Greenland (Fig. 2). The fjord system comprises the Tyrolerfjord
146 (inner fjord) and Young Sound (outer fjord), extending approximately 90 km from Tyroler River
147 to the Greenland Sea. A sill at about 45 m depth separates Young Sound from the open ocean.
148 Young Sound is 2 to 7 km wide, with an average depth of 100 m (maximum 350 m), and a total
149 surface area of ~390 km². Tidal amplitudes range from 0.8 to 1.5 m, with mean current velocities
150 of approximately 2 cm s⁻¹ (Rysgaard et al., 2003). Freshwater inputs are primarily derived from
151 Greenland Ice Sheet runoff, local glaciers, precipitation, and snowmelt from adjacent ice-free
152 terrain. The drainage basin of the Tyrolerfjord/Young Sound system spans 2846 km², of which
153 33% is glaciated.

154
155 Sampling was conducted from 12 to 31 July 2017. Sampling occurred during and immediately
156 after a period of sea ice breakup. On 15 July, ice coverage was approximately 30%, decreasing to
157 less than 10% by 16 July. Water sampling was conducted both from an inflatable boat and via
158 sea ice leads, all in close proximity to the Greenland Ecosystem Monitoring (GEM) program's
159 standard station (Fig. 2).

161 2.2 pCO₂ Measurements Using the HydroC Sensor

162 Surface water pCO₂ was measured with a CONTROS® HydroC CO₂ sensor, which utilizes a
163 membrane equilibrator coupled with a non-dispersive infrared detector. The instrument is
164 equipped with a built-in water pump that provides flow rate of 35 ml s⁻¹ across the membrane. At
165 each sampling depth, the sensor was allowed to equilibrate for 10 to 20 minutes, and values were
166 recorded once stable for at least two minutes. The sensor operates over a range of 200-1000 μatm
167 and temperatures of -2 to 35°C. Annual calibration has been conducted using a certified 400 ±
168 2% ppm CO₂ gas that was traceable to WMO standards. The sensor showed remarkable stability
169 (397-401 ppm), supporting a measurement uncertainty of ± 2 μatm.

171 2.3 pCO₂ Estimation from TA and DIC

172 In addition to direct measurements, pCO₂ was calculated from total alkalinity (TA) and dissolved
173 inorganic carbon (DIC) using the Seacarb package (Gattuso et al., 2024) in R. Due to the low
174 salinity and cold temperatures characteristic of Arctic coastal waters, no universally accepted set
175 of equilibrium constants (K1 and K2) exists. For consistency with previous studies in the region
176 (Henson et al., 2023), we used the refitted constants from (Lueker et al., 2000). The selection of

177 equilibrium constants introduces assumptions regarding seawater composition. (Raimondi et al.,
178 2019) showed that different constants can lead to discrepancies between measured and calculated
179 pCO₂ values, ranging from -3.1 to -35.8 μatm, with Lueker et al. (2000) demonstrating the best
180 internal consistency under polar conditions. Still, (Sulpis et al., 2020) found that the calculation
181 of pCO₂ from DIC and TA can lead to uncertainty up to 15% under cold conditions, which is far
182 greater than when pCO₂ is measured directly.

183

184 **2.4 Sea Ice TA and DIC Sampling**

185 TA and DIC in sea ice were assessed using three ice cores. Each core was sectioned into 5-10 cm
186 segments and sealed in gas-tight NEN/PE bags with sampling valves (Hansen et al., 2000).
187 Samples were transported in thermally insulated boxes to a nearby field laboratory. Cold (1°C)
188 deionized water of known mass and carbonate composition (10 - 30 ml) was added to each bag,
189 which was then resealed after removing air and weighted.

190

191 The samples were melted in the dark over ~48 hours. Meltwater was transferred to 12 mL
192 Exetainer vials (Labco, UK) pre-dosed with 20 μl of saturated HgCl₂ solution (5% w/v) to
193 prevent microbial alteration. DIC was measured by on Apollo SciTech®'s AS-C3 analyzer while
194 TA was determined via potentiometric titration on an Apollo SciTech AS-ALK2 total alkalinity
195 titrator (Haraldsson et al., 1997).

196

197 **2.5 Physical Parameters**

198 Vertical profiles of conductivity, temperature, and depth (CTD) were obtained using a Seabird®
199 SBE19plus CTD. On 16 July 2017, additional surface conductivity measurements were taken
200 using a Thermo Orion-Star® instrument with an Orion 013610MD conductivity cell. Surface
201 water temperatures were independently measured with a Testo® thermometer.

202

203 **2.6 Historical Data**

204 For contextual comparison, pCO₂ time series data from the Greenland Ecosystem Monitoring
205 program are also included in the analysis. pCO₂ data from 2007-2023 was measured using the
206 same HydroC CO₂ sensor in August each year.

207

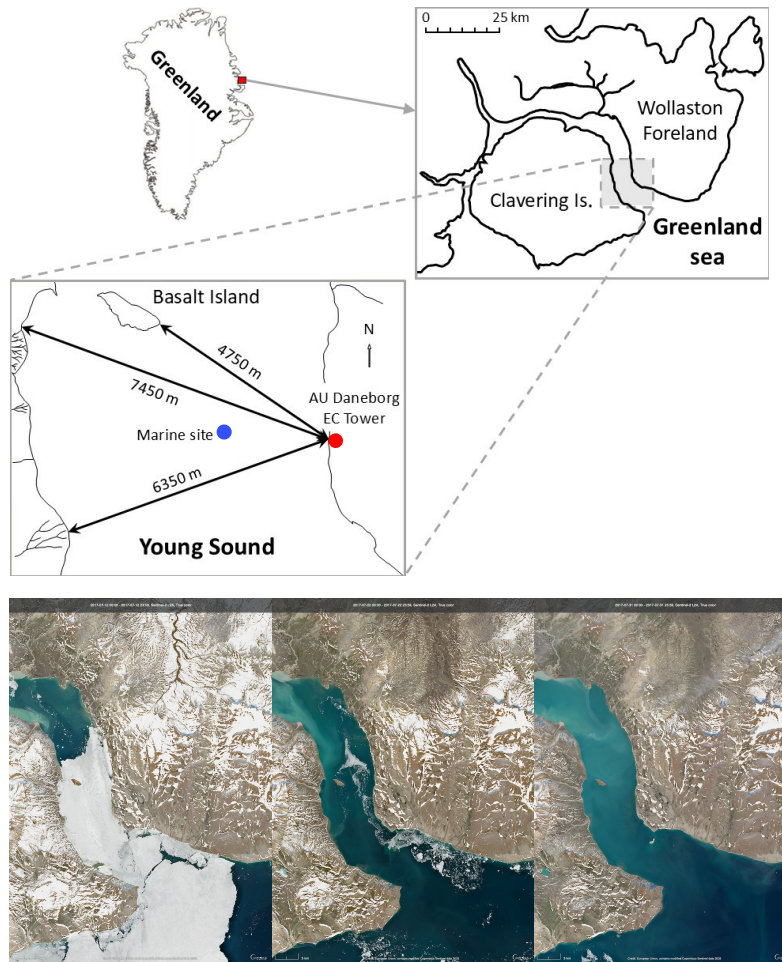
208 **2.7 Eddy Covariance**

209 Air-sea CO₂ fluxes, as well as sensible and latent heat fluxes, were estimated using
210 micrometeorological instrumentation mounted on a 3-meter mast positioned approximately 0.5
211 meters from the waterline. CO₂ concentrations were measured with a LI-COR® 7500 open-path
212 gas analyzer, and three-dimensional wind vectors were recorded using a METEK® uSonic-
213 Scientific sonic anemometer. The open-path analyzer was used at the time due to its low power
214 consumption, suitable for operation on battery systems in remote Arctic environments.
215 However, ~~F~~the authors recognize that open-path sensors over polar, marine environments can
216 lead to larger errors due to the cross-sensitivity between humidity and CO₂ for near infrared gas

217 analyzers (Blomquist et al., 2014; Landwehr et al., 2014). As a result, we do not aim to precisely
218 constrain CO₂ flux magnitudes throughout the study but provide support for the profiles
219 measured throughout this seasonal transition.
220 ~~However, the open-path analyzer was used at the time due to its low power consumption, making~~
221 ~~it suitable for operation on battery systems in remote Arctic environments.~~

222
223 To enhance reliability, we applied three complementary analysis techniques for flux estimation:
224 (1) the standard eddy covariance (EC) method using EddyPro software (Version 7.0.6, LI-COR
225 Inc., 2019); (2) the dissipation technique (DT) (Sørensen and Larsen, 2010); and (3) the ogive
226 optimization method (OGM) (Sievers et al., 2015a). Among these, the OGM was deemed most
227 robust due to its ability identify and filter out low-frequency noise, sensor dampening, and large-
228 scale turbulent motions that can bias flux measurements. These issues often introduce large
229 relative bias associated with flux measurement over surfaces characteristically exhibiting low
230 CO₂ fluxes, such as marine surfaces (Sievers et al., 2015b). OGM's superior ability to isolate
231 relevant turbulent scales and reduce contamination from mesoscale variability is based on the
232 accumulation and modelling of each cospectra over each 20 min averaging period (Fig. S1 and
233 S2). Uncertainty in CO₂ fluxes was estimated directly from the OGM procedure. The reported
234 values correspond to the standard error associated with the fitted ogive tail and reflect random
235 uncertainty in flux integration.

236



237
238

239 **Figure 2.** Map of Greenland and the sampling area at the coast of Young Sound in Northeast
240 Greenland. The red circle indicates the location of the Eddy Covariance tower while the Marine
241 sampling site (Standard Station in the Greenland Ecosystem Monitoring program) is indicated as
242 a blue circle (74.310, -20.300). Three Copernicus Sentinel true-color images of the fjord on July
243 12, 22, and 31 illustrate the transition between sea ice cover and open water.

244

245 **3 Data and results**

246

247 **3.1 CO₂ and Heat Fluxes**

248 Surface air-sea CO₂ fluxes were measured using micrometeorological techniques between July
249 16 and July 31, 2017 (Fig. 3a). However, only a limited number of flux estimates passed the
250 quality control criteria defined by OGM. This method uses a Haar wavelet analysis to assess the
251 continuity of high-frequency CO₂ and vertical wind velocity signals, rejecting fluxes when either
252 variable fails to meet spectral continuity thresholds. In addition to the automated filtering,
253 manual inspection of the cospectra was performed to evaluate fluxes that were soft-flagged by
254 the Haar analysis. Only fluxes that passed both stages of evaluation were retained for further
255 analysis and are shown in Fig. 3a (Fig. S1).

256

257 ~~Fluxes measured using eddy covariance (EC) Twenty-minute flux averages ranged from -25 to~~
258 ~~110 mmol m⁻² day⁻¹, with~~ were highly variable throughout the period of sea ice melt, exhibiting
259 both upward and downward fluxes ~~observed~~. Positive values indicate net efflux of CO₂ from the
260 ocean to the atmosphere, implying temporary oversaturation of surface waters with respect to
261 atmospheric CO₂. ~~These elevated fluxes occurred~~ EC-based effluxes were observed during and
262 shortly after the sea ice breakup period. ~~These estimates is finding~~ contrasts with prior studies in
263 Young Sound, which ~~have described~~ the fjord as a net CO₂ sink throughout the year (Sejr et al.,
264 2011). However, historic estimates are based on pCO₂ measurements from the month of August
265 and taken at 1 m depth; not from vertical pCO₂ profiles that capture salinity gradients. Similar
266 episodic outgassing events have been documented in other Arctic coastal systems under variable
267 sea ice conditions, though particularly during or following sea ice melt (Butterworth et al., 2025;
268 Else et al., 2011; Miller et al., 2011; Papakyriakou and Miller, 2011; Prytherch and Yelland,
269 2021; Sievers et al., 2015c).

270

271 In addition to CO₂ fluxes, eddy covariance measurements of sensible and latent heat fluxes were
272 also quantified during the same period and are presented in Fig. 3b and 3c. For all scalar
273 quantities, negative values represent downward fluxes directed toward the ocean surface. These
274 heat flux data provide important context for interpreting variability in CO₂ exchange, as they
275 reflect changes in atmospheric forcing and surface stratification. Corresponding meteorological
276 variables, including wind speed and air temperature, are shown in Fig. 3d-f.

277

278 The flux uncertainties shown in Fig. S3 quantify random uncertainty from the OGM integration
279 procedure. The calculated flux uncertainties are shown in Fig. S3 and illustrate CO₂ uncertainties
280 were typically below 5 mmol m⁻² d⁻¹. ~~These uncertainties were used to evaluate the robustness of~~
281 ~~positive efflux events and to interpret flux magnitudes relative to measurement precision.~~ Low
282 uncertainties during both ~~high~~ uptake and efflux events demonstrated a good signal to noise ratio
283 and provide support for the integration of fluxes during these ~~existence of~~ variable ~~uptake and~~
284 ~~outgassing conditions~~. The highest uncertainties that exceed 5 mmol m⁻² d⁻¹ corresponded to near-
285 zero fluxes, where precise flux-estimation becomes more difficult. However, these calculated
286 uncertainties do not account for potential systematic bias related to water vapor cross sensitivity,
287 which must be evaluated through other metrics.

288

289

290 3.2 Surface Water pCO₂

291 Vertical profiles of surface water pCO₂ were measured using the CONTROS® HydroC CO₂
292 sensor across three distinct periods in July 2017 (Fig. 5a-c). Each observational period
293 corresponded to different sea ice conditions: before, during and after sea ice breakup (Fig. 2).
294 These high-resolution profiles revealed substantial vertical variability within the upper 2 to 3
295 meters of the water column. Under ice-covered conditions, pCO₂ measurements were taken

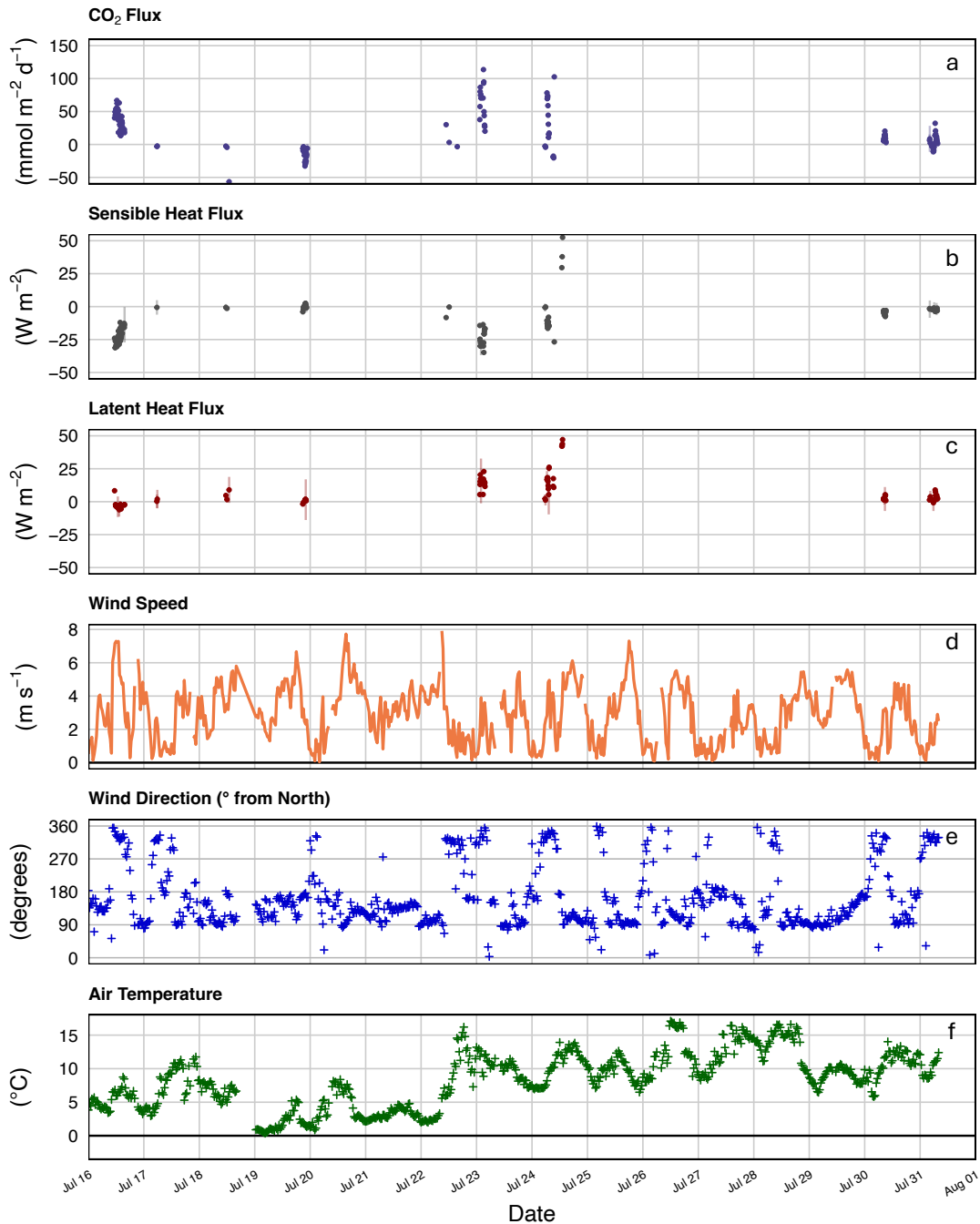
296 through an open melt pond. At this time, elevated CO₂ concentrations were observed at the very
297 surface (0.1 m), followed by a sharp decrease to approximately 1 meter depth, coinciding with
298 the ice-water interface. Below this depth, pCO₂ increased again, though remained well below
299 atmospheric concentrations (Fig. 4a).

300
301 During the period of sea ice breakup, when ice coverage ranged from approximately 30% to
302 10%, the vertical distribution of pCO₂ exhibited a similar structure. Concentrations were highest
303 near the surface, declined to a local minimum at 1 to 2 meters, and then stabilized below 3
304 meters (Fig. 4b). Following, the complete breakup of sea ice, pCO₂ showed a more gradual
305 decrease from the surface down to about 3 meters, beneath which concentrations remained
306 relatively constant (Fig. 4c). Across all three observational periods, a shallow surface layer
307 approximately 5 m thick was identified, within which most of the pCO₂ variability occurred.
308 Below this depth, pCO₂ remained relatively constant.

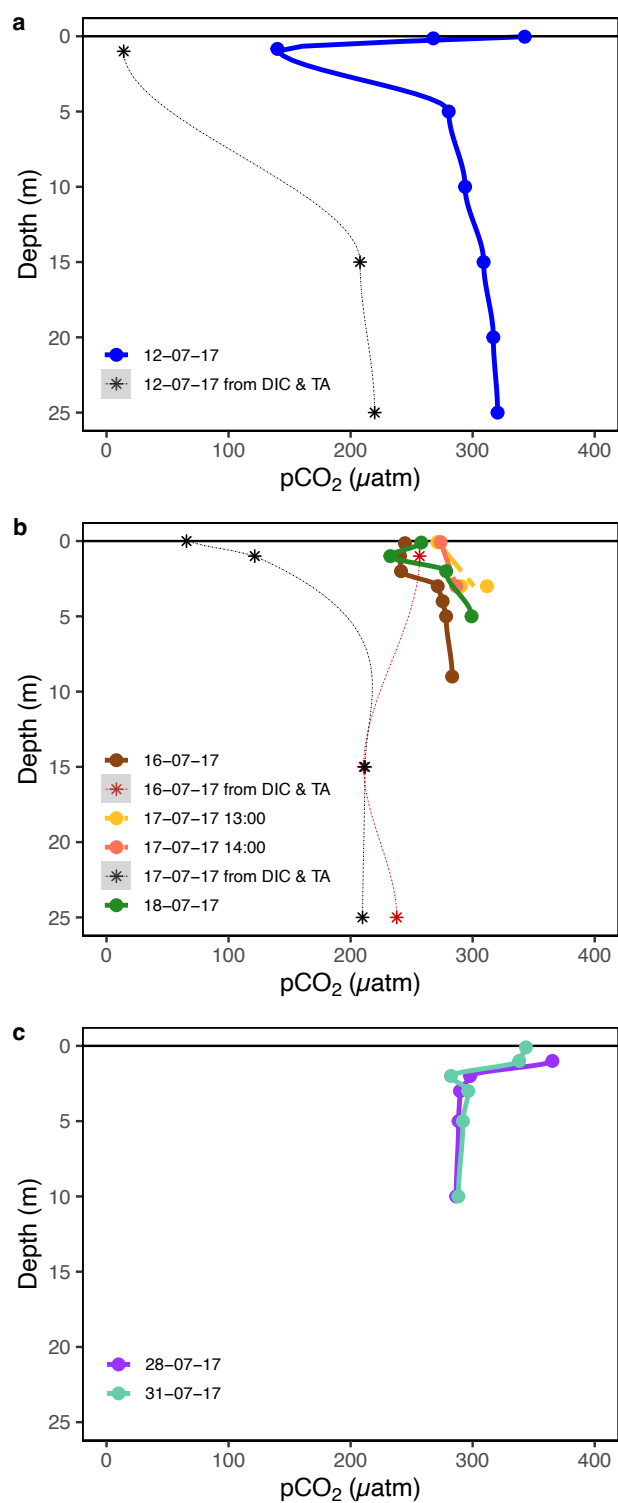
309
310 These vertical structures are consistent with strong physical stratification, likely driven by
311 freshwater input from glacial melt and surface heating. Temperature and salinity profiles
312 collected concurrently support the presence of sharp vertical gradients in the upper water
313 column, with salinity ranging from 1.4 to 29.6 PSU and temperature from -0.4°C to 6.2°C. These
314 physical profiles, shown in Fig. 5, confirm that vertical mixing was strongly suppressed during
315 the observational period.

316
317 Measurements from a different fjord in East Greenland on June 4, 2025, revealed strikingly
318 similar vertical pCO₂ heterogeneity (Fig. 6). Elevated pCO₂ at 0.1 m decreased to a minimum
319 around 1-1.5 m before increasing again and stabilizing near 3 m depth. Extreme stratification in
320 the upper few meters caused pCO₂ levels in each profile to vary by more than 100 µatm between
321 the surface and 1 m. This repeated observation of comparable vertical pCO₂ heterogeneity 8
322 years later and in a different fjord system suggest this is not an isolated phenomenon. Indeed,
323 Arctic surface stratification induces chemical changes that may influence the way we estimate
324 air-sea exchange of CO₂.

325

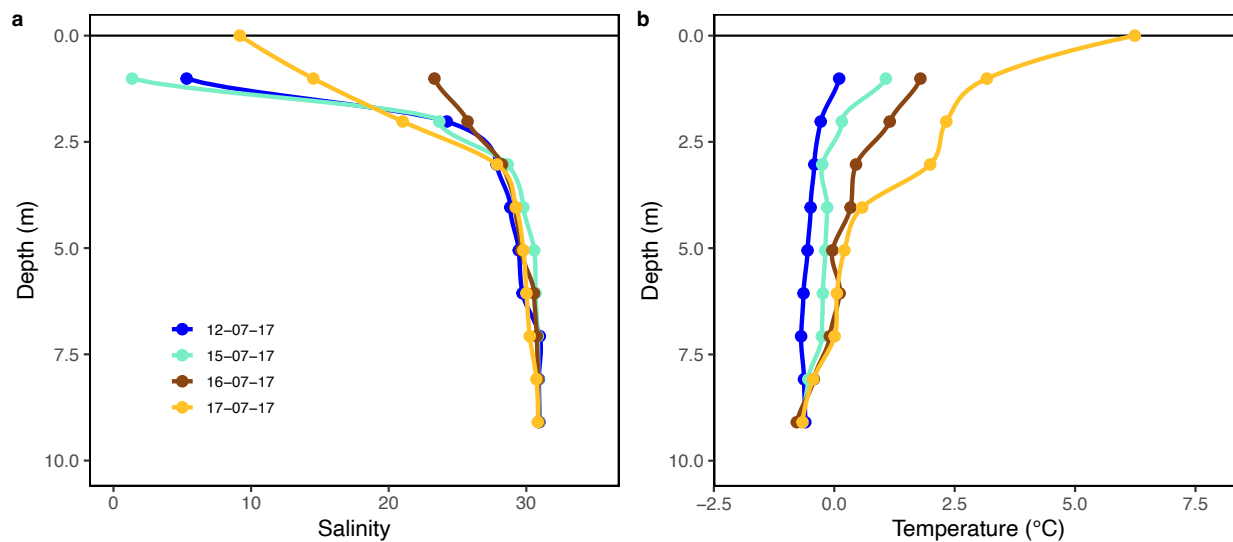


326
 327 **Figure 3.** The 5 min averages of measured fluxes and meteorological conditions over Young
 328 Sound during July 2017. This time period reflects the transition between sea ice break up (30%
 329 ice cover) and open water (no sea ice present) from 16 July 2017 to 1 August 2017. Air-sea
 330 exchange of (a) CO₂ (b) sensible heat and (c) latent heat were estimated using the ogive
 331 optimization method with estimated uncertainty shown as vertical error bars. (d) Wind speed, (e)
 332 wind direction and (f) air temperature are shown for the same period. Note: Use of an undried
 333 air-stream in the open-path CO₂ sensor likely inflates the magnitude of the illustrated CO₂ fluxes
 334 due to water vapor cross sensitivity.

336
337

338 **Figure 4.** Measured Young Sound $p\text{CO}_2$ profiles (a) prior to sea ice breakup (measured through
 339 open melt pond), (b) during sea ice breakup and (c) after sea ice break up measured through CO_2
 340 equilibration and calculation from carbonate chemistry parameters (DIC & TA).

341

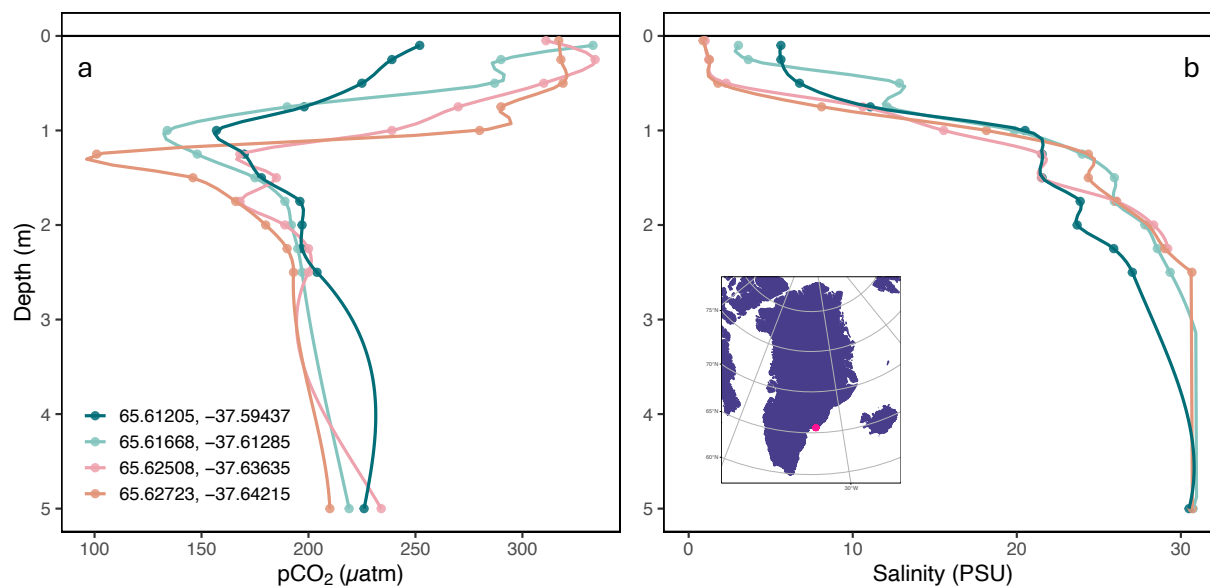


342

343

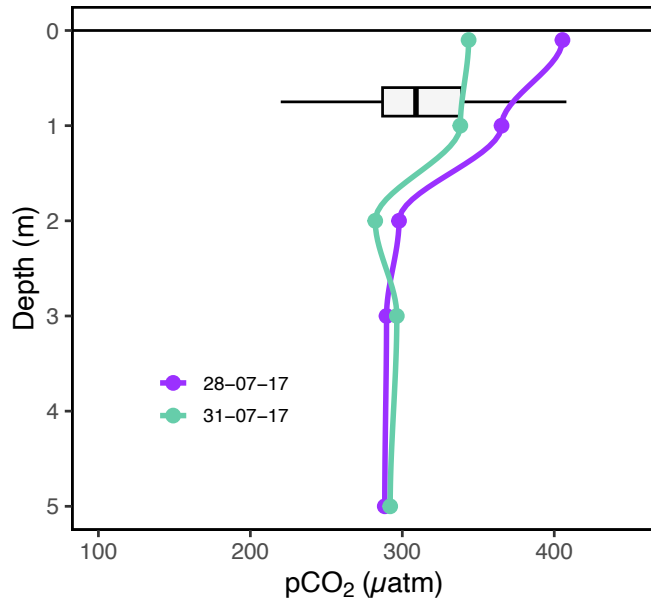
344 **Figure 5.** Measured Young Sound profiles of under-ice water and open water salinity and
345 temperature.

346



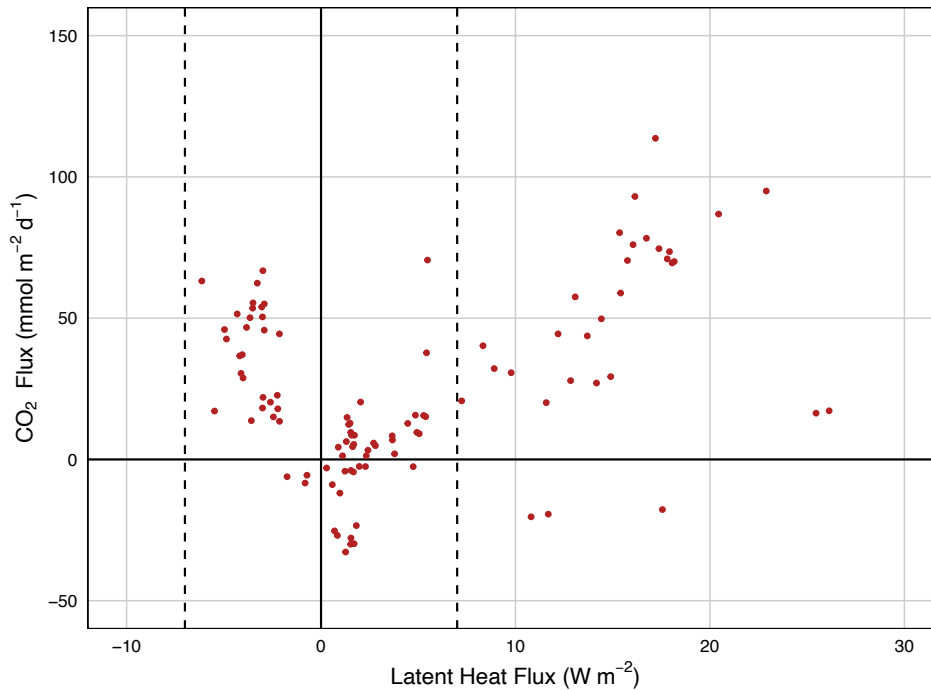
347

348 **Figure 6.** Measured $p\text{CO}_2$ (a) and salinity (b) profiles at 4 locations in Tasiilaq Bay. Profiles
349 were measured on June 4, 2025 following the method in Sejr et al. (2011).



350
351
352
353
354

Figure 7. Measured Young Sound pCO₂ profile after ice break up in 2017 compared with historical variation in pCO₂ at 1 m depth in the same location.



355
356
357
358
359
360
361

Figure 8. Relationship between CO₂ and latent heat fluxes measured using eddy covariance. Vertical dotted lines delineate the threshold ($|LE| < \sim 7 \text{ W m}^{-2}$) where Landwehr et al. (2014) found negligible water vapor-related biases in measurements from the un-dried infrared gas analyzer. Data within this range demonstrate both CO₂ uptake and effluxes, indicating that air-sea CO₂ exchange may change direction during the dynamic period of sea ice melt.

362
363
364
365
366
367
368
369
370
371
372
373
374
375
376
377
378
379
380
381
382
383
384
385
386
387
388
389
390
391
392
393
394
395
396
397
398
399
400
401

4. Discussion

Air-sea CO₂ fluxes in Arctic coastal areas are generally estimated using bulk parameterization models (Henson et al., 2024; Meire et al., 2015; Roobaert et al., 2019; Sejr et al., 2011). These models rely on several key assumptions, including unstratified surface conditions, a linear pCO₂ gradient within the diffusive boundary layer, and a vertically uniform pCO₂ profile within the mixed layer. Our observations challenge the applicability of these assumptions in Arctic coastal waters in several important ways.

4.1. Evaluating the Constant pCO₂ Assumption

Vertical pCO₂ profiles collected during July 2017 revealed pronounced non-linear behavior in the upper 3 to 5 meters of the water column (Fig. 4). This directly contradicts the assumption that the $\Delta p\text{CO}_2$ accurately represents the difference between the atmosphere and the “well-mixed bulk fluid” below the diffusive layer (Wanninkhof et al., 2009). Under ice-covered conditions, the lowest pCO₂ values (~150 ppm) were consistently observed just beneath the sea ice, with concentrations increasing with depth and stabilizing around 5 m (Fig. 4a). During the ice breakup stage, a similar pattern emerged, although the minimum pCO₂ was higher (~250 ppm).

More recent measurements from Tasiilaq Bay in June 2025 demonstrate very similar vertical pCO₂ profiles. Indeed, 4 high-resolution profiles with measurements every 0.25 m reveal the same C-shaped pCO₂ variation. Like in Young Sound, the most elevated pCO₂ levels were observed near the surface, and pCO₂ minimums occurred near 1-2 meters depth before increasing and becoming stable. This repeated observation in a different fjord system, but during the period of [sea ice](#) breakup indicates this vertical variability may be representative during stratified Arctic conditions.

Several interacting processes influence surface water chemistry during ice breakup. Low surface water pCO₂ values reflect the influence of low-salinity meltwater from snow and sea ice or glacial meltwater found in freshened Arctic waters (Geilfus et al., 2015; Henson et al., 2025). However, surface water chemistry during the ice breakup period is further complicated by processes such as ikaite (CaCO₃·6H₂O) dissolution (Miller et al., 2011; Rysgaard et al., 2013; Søgaard et al., 2013) and high under-ice primary production (Søgaard et al., 2021). Additionally, snowmelt, characterized by low pH and ionic strength (de Caritat et al., 2005), may further alter carbonate system dynamics in the upper water column.

Two mechanisms may explain the nonlinear C-shaped trend in pCO₂ observed in the top few meters. First, as demonstrated by Henson et al. (2025) mixing between glacial meltwater and seawater can result in nonlinear behavior in pCO₂, even when DIC and TA [behave-mix](#) conservatively. In such cases, initial freshwater dilution leads to dramatically reduced pCO₂, but at very low salinities, the diminished buffering capacity can cause acidification to occur and

402 pCO₂ to increase again. Although, Henson et al. focused on glacial meltwater, our results suggest
403 similar processes could occur in systems influenced by sea ice and snowmelt.

404
405 Both glacial meltwater and sea ice have low DIC concentrations and act to dilute the inorganic
406 carbon of the surface ocean (Fig. S4). However, changes in alkalinity can also impact the
407 buffering capacity of the water mixture, leading to nonlinear effects. If the meltwater has a lower
408 TA:DIC ratio than seawater, due to the absence of ikaite, acidification and a shift in carbonate
409 equilibria at very low salinities could lead to higher pCO₂ values at the surface. During July
410 2017, Young Sound showed both diluted DIC and TA levels in upper few meters, suggesting pH
411 change during sea ice break up could occur more easily (Fig. S4). Indeed, calculated pH profiles
412 indicated variable surface conditions between periods of sea ice cover and sea ice breakup (Fig.
413 S5). In this very fresh surface layer, diminished pH may elevate pCO₂ relative to waters around 1
414 m depth, where freshwater-seawater mixing ratios are more moderate and seawater buffering
415 leads to very low CO₂ concentrations.

416
417 A second, but less likely, explanation involves atmospheric equilibration of sea ice melt ponds
418 before draining into open leads. The relatively elevated pCO₂ observed at ~0.1 m depth could
419 reflect such partial equilibration. While chamber-based studies (e.g. Geilfus et al., 2012, 2015;
420 Nomura et al., 2010; Semiletov et al., 2004) have demonstrated both uptake and efflux of CO₂ in
421 melt ponds, equilibrium times between melt-pond water and atmosphere depend upon pond
422 depth, wind speed, and carbonate chemistry. For example, a 0.1 m deep pond under low wind
423 conditions (~2 m s⁻¹) may reach atmospheric equilibrium in 1-4 days. However, in our case,
424 pCO₂ values calculated from TA and DIC in melt ponds did not indicate equilibrium with the
425 atmosphere, making this explanation less likely than the freshwater mixing mechanism.

426 Nevertheless, atmospheric equilibration may play a role after the sea ice barrier is removed.
427 Elevated pCO₂ levels at the surface (0.1m) post sea ice breakup may result from the combination
428 of the chemical changes described above and from atmospheric CO₂ uptake (partial
429 equilibration) in the limited volume of this freshwater lens.

430
431 ~~Across all conditions, pCO₂ values calculated from TA and DIC using R-Seacarb were~~
432 ~~consistently lower than in situ measurements from the CONTROS sensor (Fig. 5b, c). This~~
433 ~~discrepancy supports the conclusion that chemical equilibrium is not achieved in the upper 2-4 m~~
434 ~~during the melt season in Young Sound. Standard carbonate system calculations rely on~~
435 ~~equilibrium constants that represent a set of reversible chemical reactions, assuming equilibrium~~
436 ~~has been reached for each (Emerson and Hedges, 2008). However, in a dynamic surface~~
437 ~~environment influenced by stratification, meltwater input, biological activity, and variable air-sea~~
438 ~~exchange, this assumption of a steady state is likely violated, resulting in mismatches between~~
439 ~~measured and calculated pCO₂.~~

440

~~In addition, the equilibrium constants used in these calculations are typically derived from laboratory experiments under conditions not representative of Arctic coastal waters. Most constants were determined at higher salinities and temperatures than those commonly observed during the Arctic melt season. Yet, temperature strongly impacts these thermodynamic constants (K_1 and K_2) (Cai et al., 2020). Indeed Sulpis et al. (2020) demonstrated that at temperature below 8°C, the use of constants from Lueker et al. (2000) may lead to underestimation of pCO₂, which could partially explain the discrepancies observed here.~~

As melt progresses and sea ice recedes, riverine input and vertical mixing become more influential. Yet even after ice breakup, surface waters often remain fresh due to glacial meltwater runoff, and the resulting low salinities help maintain stratification. In August 2017, vertical structure remained pronounced, with elevated pCO₂ at 0.1 m which stabilized below ~3 m. In other words, near-surface conditions remained decoupled from deeper waters. This persistent shallow layer, characterized by low salinity, higher temperature, and elevated pCO₂, suppresses gas exchange with the colder, more undersaturated water below, consistent with observations by Dong et al. (2021). In such environments, bulk flux models that assume homogeneity and linear gradients are likely to yield biased or inaccurate estimates.

To place these 2017 measurements in historical context, we examined long-term surface water pCO₂ data collected at 0.5-1 m depth by the Greenland Ecosystem Monitoring (GEM) program between 2007 and 2023. These data, measured using consistent protocols, are presented in Fig. 7 alongside our open-water profiles. Over the 17-year record, August pCO₂ concentrations at ~1 m depth had ranged from 220 to 408 μatm and had consistently remained below atmospheric levels. This apparent stability has contributed to the perception of sustained CO₂ uptake throughout the summer season.

However, the high-resolution vertical profiles obtained during the 2017 field campaign challenge this assumption. Elevated pCO₂ levels confined to the uppermost meter of the water column may go undetected in standard monitoring approaches that rely on fixed-depth sampling. These results suggest that short-lived ~~but significant~~ episodes of CO₂ outgassing can occur during rapid environmental transitions such as sea ice breakup. Consequently, existing sampling protocols may underestimate surface variability and bias flux estimates, especially in stratified conditions where near-surface chemistry is decoupled from subsurface layers.

4.2. Evaluating Bulk Model Flux Estimates

To assess whether bulk models are suitable for estimating CO₂ fluxes in an Arctic fjord influenced by sea ice and snow melt, we calculated fluxes using seawater pCO₂ measurements from multiple depths and two gas transfer velocity parameterizations. Specifically, we computed fluxes throughout July using pCO₂ measured at 0.1, 1, 2, and 4 m. To estimate the surface (interface) pCO₂ at 0 m, we adjusted the 1 m pCO₂ measurements to a derived skin temperature (Table 1), estimated from sensible heat fluxes (Fig. 3b) for the thermal skin effect based on skin

480 ~~temperature derived from sensible heat flux data (Fig. 3b)~~, following the parameterization of
481 Smedman et al. (2007). Accounting for this skin layer correction is critical, as Woolf et al.
482 (2016) demonstrated that neglecting the thermal skin and relying only on bulk sea surface
483 temperature can introduce significant errors in flux estimates.

484
485 The resulting calculations (Table 1) show that estimated CO₂ fluxes vary significantly depending
486 on the depth of the pCO₂ measurement. Notably, fluxes derived from 0.1 m differ markedly from
487 those based on deeper values. Since many studies rely on pCO₂ measured at a fixed depth (often
488 at 1 m or at a ship's seawater intake below 5 m), these results underscore the potential for
489 misrepresentation of flux direction and magnitude due to vertical heterogeneity in surface water
490 chemistry.

491
492 Measured fluxes from eddy covariance (Fig. 3a) also exhibited large temporal variability. While
493 micrometeorological methods integrate fluxes over a horizontal footprint, bulk flux models rely
494 on single point pCO₂ gradients between air and water. Consequently, under heterogeneous or
495 partially ice-covered conditions, the two methods are unlikely to yield identical results.

496 However, ~~a qualitative comparison between the two approaches remains informative. meaningful~~
497 ~~comparison is still possible.~~ Notably, agreement between micrometeorological and bulk model
498 estimates was only observed in late July, and only when in situ pCO₂ was ~~corrected for~~
499 ~~thenormalized to the derived~~ skin temperature. This aligns with the conclusions of Woolf et al.
500 (2016) and Ford et al. (2024), who suggest that using skin-adjusted pCO₂ may improve flux
501 estimates. Accurate application of this correction would require either direct measurements of
502 skin temperature when sampling for the bulk method or high-resolution modeling of heat fluxes.

503
504 However, this agreement between methods did not hold before or immediately after ice breakup.
505 During these periods, micrometeorological methods indicated episodes of large upward fluxes
506 (~~48 mmol m⁻² d⁻¹~~), while bulk model estimates suggested downward fluxes (-14 mmol m⁻² d⁻¹).
507 Although both methods yielded comparable magnitudes for downward fluxes, only the
508 micrometeorological approach captured large upward events that could not be reconciled with
509 ~~explained by~~ surface water pCO₂ profiles alone.

510
511 Measurements from both Young Sound and Tasiilaq demonstrate that during sea ice breakup,
512 pCO₂ levels are most elevated at the surface. This may be linked to acidification of the most
513 freshened 0.5 m and a shift in the marine carbonate system, or partial equilibration due to air-sea
514 gas transfer. If ~~this acidified freshwater lens the air-sea boundary layer~~ warms, for instance, due
515 to solar radiation, pCO₂ may rise ~~rapidly~~ leading to oversaturation relative to atmospheric
516 concentrations. Indeed, when pCO₂ measurements on July 31 were corrected for skin
517 temperature, to estimate pCO₂ at the boundary layer, they ~~revealed-suggested~~ a transition from
518 undersaturation to oversaturation (Table 1). While we did not directly observe this oversaturation
519 in the vertical profiles, this likely reflects the inability to sample at the very surface layer.

520 Moreover, profile measurements represent only single points in a system characterized by strong
521 spatial and temporal variability during this seasonal transition. Nevertheless, the occurrence of
522 C-shaped pCO₂ profiles during sea ice breakup may help explain the ~~observed-apparent~~I think
523 reversal of flux direction ~~captured-suggested~~ by the micrometeorological approach.

524
525 Another potential explanation for the elevated CO₂ efflux that cannot be ~~fully~~-discounted
526 involves cross-sensitivity between water vapor and CO₂ in open-path NDIR sensors (Blomquist
527 et al., 2014; Landwehr et al., 2014). Although the OGM processing method is designed to
528 minimize humidity-induced artifacts and large-scale turbulent motions, it cannot entirely remove
529 them. While many of the extreme eddy covariance measurements from Young Sound are likely
530 influenced by humidity-CO₂ cross sensitivity, ~~However~~, several lines of evidence indicate that
531 ~~the-some~~ positive CO₂ fluxes are-may not solely be-an attributed to this artifact-of water vapor.
532 In their comparative methodological study, Landwehr et al. (2014) identified large biases in
533 open-path NDIR sensors related to water-vapor fluctuations, but reported agreement between
534 sensors operating with dried and undried air streams during periods of low latent heat flux ($|LE|$
535 $\leq 7 \text{ W m}^{-2}$), where humidity-related bias was negligible. When examining the subset of Young
536 Sound data below this threshold, eddy covariance measurements exhibit both positive and
537 negative CO₂ flux estimates (Fig. 8). Additionally, elevated CO₂ concentrations occur across a
538 wide range of relative humidities (Fig. S6)~~Elevated CO₂ concentrations occurred during some,~~
539 ~~but not all, periods of high relative humidity, and extended intervals with similarly high humidity~~
540 ~~exhibited low CO₂ levels (Fig. S6).~~ Moreover, positive CO₂ fluxes were observed even during
541 negative latent heat flux events (Fig. S7a), which is inconsistent with a purely humidity-driven
542 bias. ~~In addition, CO₂ fluxes exhibited a strong negative relationship with sensible heat flux (Fig.~~
543 ~~S7b), consistent with physical air-sea exchange processes in marine environments.~~ Taken
544 together, these patterns support the interpretation that ~~the-observed-some of the measured~~
545 effluxes may represent real air-sea CO₂ exchange rather than ~~being-dominated-by~~solely resulting
546 from cross-sensitivity artifacts. However, definitive quantification using this experimental setup
547 remains impossible and Still, future studies using closed-path sensors during Arctic seasonal
548 transitions are ~~encouraged-required~~ to ~~verify-the-precise~~robustly constrain the magnitude of CO₂
549 outgassing and uptake.

550
551 Overall, these findings echo those of Miller et al. (2019), who reported pronounced spatial
552 heterogeneity in Arctic coastal pCO₂ and large differences in estimated flux depending on the
553 sampling depth. The broader implications of this heterogeneity for seasonal or regional flux
554 estimates remain unclear. However, if fluxes are upscaled from sparse, single-point
555 measurements (e.g., once per month, as in Laruelle et al., 2014), substantial errors may result due
556 to unrecognized spatial and temporal variability. Thus, our results emphasize the need for
557 continuous, high-resolution observations of air-sea CO₂ fluxes, particularly in Arctic coastal
558 systems affected by stratification and meltwater input. These observations ~~are-will be~~ essential

559 for refining flux parameterizations, reducing uncertainty in carbon budget estimates, and
 560 improving the representation of Arctic shelf systems in global carbon models.

561
 562 **Table 1.** CO₂ fluxes calculated based on pCO₂ measured at the different depth. The fluxes are
 563 calculated using the bulk model of Ho et al., 2006 and Nightingale et al. (2000). We have used
 564 locally measured wind speeds for the calculations to match flux measurements captured by eddy
 565 covariance. ~~The pCO₂ at 0 m is calculated from the pCO₂ measured at 1 m and then adjusted to~~
 566 ~~the skin temperature, which is derived the measured heat fluxes.~~

567

Date	Depth (m)	Temperature (°C)	Salinity (psu)	pCO ₂ (µatm)	Wind Speed (m s ⁻¹)	Ho (2006)	Nightingale (2000)	Eddy Covariance
						Flux (mmol CO ₂ m ⁻² day ⁻¹)	Flux (mmol CO ₂ m ⁻² day ⁻¹)	Flux (mmol CO ₂ m ⁻² day ⁻¹)
16-Jul	0.0	3.0 [‡]	23	252 [‡]	6.8	-14.88	-13.69	48.3
16-Jul	0.1	3.0	23	244	6.8	-15.78	-14.52	
16-Jul	1.0	1.8	26	240	6.8	-16.12	-14.83	
16-Jul	2.0	1.1	28	241	6.8	-15.93	-14.66	
16-Jul	4.0	0.3	29	275	6.8	-12.19	-11.21	
18-Jul	0.0	6.0 [‡]	7	262 [‡]	3.3	-3.45	-3.38	-3.49
18-Jul	0.1	4.3	7	244	3.3	-3.98	-3.90	
18-Jul	1.0	3.2	14	233	3.3	-4.20	-4.11	
18-Jul	2.0	2.3	21	278	3.3	-2.86	-2.79	
18-Jul	4.0	0.6	29	295	3.3	-2.34	-2.29	
28-Jul	0.0	10.0 [‡]	15	415 [‡]	2.5	0.53	0.54	—
28-Jul	0.1	10.0	15	405	2.5	0.38	0.38	
28-Jul	1.0	7.0	21	365	2.5	-0.22	-0.23	
28-Jul	2.0	5.0	27	282	2.5	-1.43	-1.45	
28-Jul	4.0	2.0	30	290	2.5	-1.32	-1.34	
31-Jul	0.0	12.0 [‡]	15	401 [‡]	2.0	0.20	0.21	5.07
31-Jul	0.1	10.0	15	343	2.0	-0.36	-0.38	
31-Jul	1.0	8.0	21	338	2.0	-0.40	-0.42	
31-Jul	2.0	5.0	27	282	2.0	-0.92	-0.97	
31-Jul	4.0	2.0	30	294	2.0	-0.81	-0.85	

568

569 † Denotes skin temperatures derived from heat fluxes. ‡ Denotes pCO₂ values estimated from
570 measurements at 1 m depth and adjusted to derived skin temperatures.

573 **5 Conclusions**

574
575 During the summer thaw, carbon chemistry and pCO₂ dynamics in Arctic coastal surface waters
576 are significantly altered by the combined effects of snow and sea ice melt, terrestrial runoff, and
577 biological activity. These influences lead to substantial variability in surface temperature, pH,
578 dissolved inorganic carbon (DIC), and total alkalinity (TA), ultimately disrupting carbonate
579 system equilibrium in the upper water column. As a result, estimating air-sea CO₂ fluxes using
580 traditional bulk models becomes highly uncertain during this period.

581
582 The sea ice breakup period, typically lasting 2-4 weeks, represents a particularly dynamic and
583 complex phase in the annual cycle. Despite its brevity, this phase may have a disproportionate
584 influence on total summer CO₂ uptake, given that open-water conditions in high Arctic fjords are
585 limited to only 80-120 days per year (Sejr et al., 2011).

586
587 Improved flux estimates will require more detailed and spatially resolved investigations aimed at
588 developing and validating gas exchange parameterizations tailored to the highly stratified and
589 ice-affected conditions of Arctic fjords. In particular, new approaches are needed to estimate gas
590 transfer velocities over waters influenced by snow and sea ice melt. Exchange rates depend not
591 only on the pCO₂ gradient between the atmosphere and surface water, but also on rapid,
592 nonlinear changes in surface water chemistry driven by the composition and volume of
593 meltwater and runoff.

594
595 Once more suitable parameterizations for gas transfer velocity are established, accurate flux
596 estimation will also require knowledge of the depth at which surface water pCO₂ becomes
597 vertically homogeneous. Profiling pCO₂ in the upper water column is therefore essential to
598 identify this depth and to constrain surface flux estimates reliably.

599
600 Several eddy covariance studies in other arctic environments report variable uptake and efflux of
601 CO₂ during the sea ice breakup period (e.g. Butterworth et al., 2025). Our study revealed large
602 upward CO₂ fluxes using the Similarly, eddy covariance measurements (OGM) method, in
603 Young Sound particularly during the ice breakup period—exhibited both positive and negative
604 CO₂ flux estimates during this seasonal transition. However, these upward fluxes that were not
605 captured by the bulk model. These variable and sometimes conflicting dataset events underscore
606 the need for studies that integrate continuous, direct CO₂ flux measurements with detailed
607 observations of surface water carbonate chemistry, atmospheric forcing, skin temperature, and
608 turbulence at the air-ice-water interface.

610 Such integrated measurements are critical to improving our understanding of the frequency,
611 drivers, and net effect of **episodic** upward CO₂ fluxes in Arctic coastal systems. Ultimately, this
612 knowledge is essential to accurately quantify the seasonal and regional uptake of atmospheric
613 CO₂ in the rapidly changing Arctic.

617 **Acknowledgments**

618 This study is a contribution to the GreenFeedback project (Greenhouse gas fluxes and earth
619 system feedbacks, Grant agreement: 101056921), funded by the European Union under the
620 Horizon Europe program, who also supported L.L.S and H.C.H's involvement. H.C.H. was
621 additionally funded by the AUFF (Aarhus Universitets Forskningsfond, project no. AUFF-F-
622 2021-7-7) as part of his PhD. S.R. was funded by Aage V Jensens Fonde (grant no. AVJF21-
623 3012) and the Danish National Research Foundation (grant no. DNRF 185). MKS was funded by
624 the POMP project (Horizon Europe grant: 101136875) and the Connecting the Dots project
625 (Villum Foundation grant: 50110) D.H.S received financial support from the Greenland Climate
626 Research Centre (GCRC), Greenland Institute of Natural Resources. The study also received
627 financial support from The Danish Ministry of Climate, Energy and Utilities, Programme for
628 Arctic Climate, (project: Drivhusgas-observationer i Arktis (ObsArktis), 2017). Furthermore we
629 received support from The Arctic Research Centre, Aarhus University and Greenland Institute of
630 Natural Science. The authors especially wish to thank Egon Randa Frandsen, who assisted with
631 the logistics and the additional measurements in Young Sound. Additionally, the authors would
632 like to recognize the students in the EnCHil Nordic master program, who participated in taking
633 the Tasiilaq measurements. This work is a contribution to the Arctic Science Partnership (ASP)
634 and the MarinBasis component of the Greenland Ecosystem Monitoring Program.

636 **Author Contribution**

637 Conceptualization: LLS. Formal analysis, writing – original draft preparation: HCH. Funding
638 acquisition: LLS, SR, MKS, TP. Investigation: DS, BJ, KL, TP, MKS, JS, SR, LLS. Writing –
639 review and editing: DS, TP, MKS, SR, LLS. All the authors have read and agreed to the
640 published version of the paper.

642 **Data Availability Statement**

643 Vertical profiles from both Greenlandic fjords can be found in the Zenodo data repository:
644 <https://doi.org/10.5281/zenodo.17471918>

646 **Competing interests**

647 The authors declare no competing interests.

650
651
652
653
654
655
656
657
658
659
660
661
662
663
664
665
666
667
668
669
670
671
672
673
674
675
676
677
678
679
680
681
682
683
684
685
686
687
688
689
690
691

References

- Ahmed, M. M. M., Else, B. G. T., Capelle, D., Miller, L. A., and Papakyriakou, T.: Underestimation of surface p CO₂ and air-sea CO₂ fluxes due to freshwater stratification in an Arctic shelf sea, Hudson Bay, *Elementa: Science of the Anthropocene*, 8, 084, <https://doi.org/10.1525/elementa.084>, 2020.
- Arrigo, K. R. and van Dijken, G. L.: Continued increases in Arctic Ocean primary production, *Progress in Oceanography*, 136, 60–70, <https://doi.org/10.1016/j.pocean.2015.05.002>, 2015.
- Bates, N. R. and Mathis, J. T.: The Arctic Ocean marine carbon cycle: evaluation of air-sea CO₂ exchanges, ocean acidification impacts and potential feedbacks, *Biogeosciences*, 6, 2433–2459, 2009.
- Blomquist, B. W., Huebert, B. J., Fairall, C. W., Bariteau, L., Edson, J. B., Hare, J. E., and McGillis, W. R.: Advances in Air–Sea CO_2 Flux Measurement by Eddy Correlation, *Boundary-Layer Meteorol.*, 152, 245–276, <https://doi.org/10.1007/s10546-014-9926-2>, 2014.
- Burgers, T. M., Miller, L. A., Thomas, H., Else, B. G. T., Gosselin, M., and Papakyriakou, T.: Surface Water CO₂ Variations and Sea–Air CO₂ Fluxes During Summer in the Eastern Canadian Arctic, *J. Geophys. Res. Oceans*, 122, 9663–9678, <https://doi.org/10.1002/2017jc013250>, 2017.
- Butterworth, B. J., Else, B. G. T., Brown, K. A., Mundy, C. J., Williams, W. J., Rotermund, L. M., and de Boer, G.: Annual carbon dioxide flux over seasonal sea ice in the Canadian Arctic, *EGU sphere*, 1–30, <https://doi.org/10.5194/egusphere-2025-1802>, 2025.
- de Caritat, P., Hall, G., Gislason, S., Belsey, W., Braun, M., Goloubeva, N. I., Olsen, H. K., Scheie, J. O., and Vaive, J. E.: Chemical composition of arctic snow: concentration levels and regional distribution of major elements, *Science of The Total Environment*, 336, 183–199, <https://doi.org/10.1016/j.scitotenv.2004.05.031>, 2005.
- Dai, M., Su, J., Zhao, Y., Hofmann, E. E., Cao, Z., Cai, W.-J., Gan, J., Lacroix, F., Laruelle, G. G., Meng, F., Müller, J. D., Regnier, P. A. G., Wang, G., and Wang, Z.: Carbon Fluxes in the Coastal Ocean: Synthesis, Boundary Processes, and Future Trends, *Annu. Rev. Earth Planet. Sci.*, 50, 593–626, <https://doi.org/10.1146/annurev-earth-032320-090746>, 2022.
- Dong, Y., Yang, M., Bakker, D. C. E., Liss, P. S., Kitidis, V., Brown, I., Chierici, M., Fransson, A., and Bell, T. G.: Near-Surface Stratification Due to Ice Melt Biases Arctic Air–Sea CO₂ Flux Estimates, *Geophysical Research Letters*, 48, <https://doi.org/10.1029/2021GL095266>, 2021.
- Else, B. G. T., Papakyriakou, T. N., Galley, R. J., Drennan, W. M., Miller, L. A., and Thomas, H.: Wintertime CO₂ fluxes in an Arctic polynya using eddy covariance: Evidence for enhanced air-sea gas transfer during ice formation, *J. Geophys. Res.*, 116, C00G03, <https://doi.org/10.1029/2010JC006760>, 2011.
- Ford, D. J., Shutler, J. D., Blanco-Sacristán, J., Corrigan, S., Bell, T. G., Yang, M., Kitidis, V., Nightingale, P. D., Brown, I., Wimmer, W., Woolf, D. K., Casal, T., Donlon, C., Tilstone, G. H., and Ashton, I.: Enhanced ocean CO₂ uptake due to near-surface temperature gradients, *Nat. Geosci.*, 17, 1135–1140, <https://doi.org/10.1038/s41561-024-01570-7>, 2024.

692 Garbe, C. S., Rutgersson, A., Boutin, J., de Leeuw, G., Delille, B., Fairall, C. W., Gruber, N., Hare, J., Ho, D. T.,
693 Johnson, M. T., Nightingale, P. D., Pettersson, H., Piskozub, J., Sahlée, E., Tsai, W., Ward, B., Woolf, D. K., and
694 Zappa, C. J.: Transfer Across the Air-Sea Interface, in: Ocean-Atmosphere Interactions of Gases and Particles,
695 edited by: Liss, P. S. and Johnson, M. T., Springer, Berlin, Heidelberg, 55–112, [https://doi.org/10.1007/978-3-642-](https://doi.org/10.1007/978-3-642-25643-1_2)
696 25643-1_2, 2014.

697 Gattuso, J.-P., Epitalon, J.-M., Lavigne, H., Orr, J., Gentili, B., Hagens, M., Hofmann, A., Mueller, J.-D., Proye, A.,
698 Rae, J., and Soetaert, K.: seacarb: Seawater Carbonate Chemistry, 2024.

699 Geilfus, N.-X., Carnat, G., Papakyriakou, T., Tison, J.-L., Else, B., Thomas, H., Shadwick, E., and Delille, B.:
700 Dynamics of pCO₂ and related air-ice CO₂ fluxes in the Arctic coastal zone (Amundsen Gulf, Beaufort Sea), *J.*
701 *Geophys. Res.*, 117, n/a-n/a, <https://doi.org/10.1029/2011JC007118>, 2012.

702 Geilfus, N.-X., Galley, R. J., Crabeck, O., Papakyriakou, T., Landy, J., Tison, J.-L., and Rysgaard, S.: Inorganic
703 carbon dynamics of melt-pond-covered first-year sea ice in the Canadian Arctic, *Biogeosciences*, 12, 2047–2061,
704 <https://doi.org/10.5194/bg-12-2047-2015>, 2015.

705 Granskog, M. A., Kuzyk, Z. Z. A., Azetsu-Scott, K., and Macdonald, R. W.: Distributions of runoff, sea-ice melt
706 and brine using $\delta^{18}\text{O}$ and salinity data — A new view on freshwater cycling in Hudson Bay, *Journal of Marine*
707 *Systems*, 88, 362–374, <https://doi.org/10.1016/j.jmarsys.2011.03.011>, 2011.

708 Hansen, J. W., Thamdrup, B., and Jørgensen, B. B.: Anoxic incubation of sediment in gas-tight plastic bags: a
709 method for biogeochemical process studies, *Marine Ecology Progress Series*, 208, 273–282, 2000.

710 Haraldsson, C., Anderson, L. G., Hassellöv, M., Hulth, S., and Olsson, K.: Rapid, high-precision potentiometric
711 titration of alkalinity in ocean and sediment pore waters, *Deep Sea Research Part I: Oceanographic Research Papers*,
712 44, 2031–2044, [https://doi.org/10.1016/S0967-0637\(97\)00088-5](https://doi.org/10.1016/S0967-0637(97)00088-5), 1997.

713 Henson, H. C., Holding, J. M., Meire, L., Rysgaard, S., Stedmon, C. A., Stuart-Lee, A., Bendtsen, J., and Sejr, M.:
714 Coastal freshening drives acidification state in Greenland fjords, *Science of The Total Environment*, 855, 158962,
715 <https://doi.org/10.1016/j.scitotenv.2022.158962>, 2023.

716 Henson, H. C., Sejr, M., Meire, L., Sørensen, L. L., Winding, M. H. S., and Holding, J. M.: Resolving Heterogeneity
717 in CO₂ Uptake Potential in the Greenland Coastal Ocean, *Journal of Geophysical Research: Biogeosciences*, 129,
718 e2024JG008246, <https://doi.org/10.1029/2024JG008246>, 2024.

719 Henson, H. C., Puts, I. C., Sejr, M. K., Sørensen, L. L., and Holding, J. M.: Glacial meltwater increases coastal
720 carbon dioxide uptake and sensitivity to biogeochemical change, *Commun Earth Environ*, 6, 687,
721 <https://doi.org/10.1038/s43247-025-02685-4>, 2025.

722 Jørgensen, H. E., Sørensen, L. L., and Larsen, S. E.: A Simple Model of Chemistry Effects on the Air-Sea CO₂
723 Exchange Coefficient, *Journal of Geophysical Research: Oceans*, 125, e2018JC014808,
724 <https://doi.org/10.1029/2018JC014808>, 2020.

725 Landwehr, S., Miller, S. D., Smith, M. J., Saltzman, E. S., and Ward, B.: Analysis of the PKT correction for direct
726 CO₂ flux measurements over the ocean, *Atmospheric Chemistry and Physics*, 14, 3361–3372,
727 <https://doi.org/10.5194/acp-14-3361-2014>, 2014.

728 Laruelle, G. G., Lauerwald, R., Pfeil, B., and Regnier, P.: Regionalized global budget of the CO₂ exchange at the
729 air-water interface in continental shelf seas, *Global Biogeochemical Cycles*, 28, 1199–1214,
730 <https://doi.org/10.1002/2014GB004832>, 2014.

731 Liss, P. S. and Slater, P. G.: Flux of Gases across the Air-Sea Interface, *Nature*, 247, 181–184,
732 <https://doi.org/10.1038/247181a0>, 1974.

- 733 Lueker, T. J., Dickson, A. G., and Keeling, C. D.: Ocean pCO₂ calculated from dissolved inorganic carbon,
734 alkalinity, and equations for K₁ and K₂: validation based on laboratory measurements of CO₂ in gas and seawater at
735 equilibrium, *Marine Chemistry*, 70, 105–119, [https://doi.org/10.1016/s0304-4203\(00\)00022-0](https://doi.org/10.1016/s0304-4203(00)00022-0), 2000.
- 736 Meire, L., Søgaard, D. H., Mortensen, J., Meysman, F. J. R., Soetaert, K., Arendt, K. E., Juul-Pedersen, T., Blicher,
737 M. E., and Rysgaard, S.: Glacial meltwater and primary production are drivers of strong
738 CO₂ uptake in fjord and coastal waters adjacent to the Greenland Ice Sheet,
739 *Biogeosciences*, 12, 2347–2363, <https://doi.org/10.5194/bg-12-2347-2015>, 2015.
- 740 Meire, L., Mortensen, J., Meire, P., Juul-Pedersen, T., Sejr, M. K., Rysgaard, S., Nygaard, R., Huybrechts, P., and
741 Meysman, F. J. R.: Marine-terminating glaciers sustain high productivity in Greenland fjords, *Glob Change Biol*, 23,
742 5344–5357, <https://doi.org/10.1111/gcb.13801>, 2017.
- 743 Miller, L. A., Papakyriakou, T. N., Collins, R. E., Deming, J. W., Ehn, J. K., Macdonald, R. W., Mucci, A., Owens,
744 O., Raudsepp, M., and Sutherland, N.: Carbon dynamics in sea ice: A winter flux time series, *J. Geophys. Res.*, 116,
745 C02028, <https://doi.org/10.1029/2009JC006058>, 2011.
- 746 Miller, L. A., Burgers, T. M., Burt, W. J., Granskog, M. A., and Papakyriakou, T. N.: Air-Sea CO₂ Flux Estimates
747 in Stratified Arctic Coastal Waters: How Wrong Can We Be?, *Geophys. Res. Lett.*, 46, 235–243,
748 <https://doi.org/10.1029/2018gl080099>, 2019.
- 749 Nomura, D., Yoshikawa-Inoue, H., Toyota, T., and Shirasawa, K.: Effects of snow, snowmelting and refreezing
750 processes on air–sea-ice CO₂ flux, *Journal of Glaciology*, 56, 262–270,
751 <https://doi.org/10.3189/002214310791968548>, 2010.
- 752 Papakyriakou, T. and Miller, L.: Springtime CO₂ exchange over seasonal sea ice in the Canadian Arctic
753 Archipelago, *Annals of Glaciology*, 52, 215–224, <https://doi.org/10.3189/172756411795931534>, 2011.
- 754 Perovich, D., Meier, W., Tschudi, M., Hendricks, S., Petty, A. A., Divine, D., Farrell, S., Gerland, S., Haas, C.,
755 Kaleschke, L., Pavlova, O., Ricker, R., Tian-Kunze, X., Webster, M., and Wood, K.: Arctic Report Card 2020: Sea
756 Ice, 2020.
- 757 Prytherch, J. and Yelland, M. J.: Wind, Convection and Fetch Dependence of Gas Transfer Velocity in an Arctic
758 Sea-Ice Lead Determined From Eddy Covariance CO₂ Flux Measurements, *Global Biogeochemical Cycles*, 35,
759 e2020GB006633, <https://doi.org/10.1029/2020GB006633>, 2021.
- 760 Raimondi, L., Matthews, J. B. R., Atamanchuk, D., Azetsu-Scott, K., and Wallace, D. W. R.: The internal
761 consistency of the marine carbon dioxide system for high latitude shipboard and *in situ* monitoring, *Marine*
762 *Chemistry*, 213, 49–70, <https://doi.org/10.1016/j.marchem.2019.03.001>, 2019.
- 763 Roobaert, A., Laruelle, G. G., Landschützer, P., Gruber, N., Chou, L., and Regnier, P.: The Spatiotemporal
764 Dynamics of the Sources and Sinks of CO₂ in the Global Coastal Ocean, *Global Biogeochemical Cycles*, 33, 1693–
765 1714, <https://doi.org/10.1029/2019GB006239>, 2019.
- 766 Rysgaard, S., Vang, T., Stjernholm, M., Rasmussen, B., Windelin, A., and Kiilsholm, S.: Physical Conditions,
767 Carbon Transport, and Climate Change Impacts in a Northeast Greenland Fjord, *Arctic, Antarctic, and Alpine*
768 *Research*, 35, 301–312, [https://doi.org/10.1657/1523-0430\(2003\)035%255B0301:PCCTAC%25D2.0.CO;2](https://doi.org/10.1657/1523-0430(2003)035%255B0301:PCCTAC%25D2.0.CO;2), 2003.
- 769 Rysgaard, S., Søgaard, D. H., Cooper, M., Pu´co, M., Lennert, K., Papakyriakou, T. N., Wang, F.,
770 Geilfus, N. X., Glud, R. N., Ehn, J., McGinnis, D. F., Attard, K., Sievers, J., Deming, J. W., and Barber, D.: Ikaite
771 crystal distribution in winter sea ice and implications for CO₂ system dynamics, *The Cryosphere*, 7, 707–718,
772 <https://doi.org/10.5194/tc-7-707-2013>, 2013.

773 Sejr, Krause-Jensen, D., Rysgaard, S., Sørensen, L. L., Christensen, P. B., and Glud, R. N.: Air—sea flux of CO₂ in
774 arctic coastal waters influenced by glacial melt water and sea ice, *Tellus B: Chemical and Physical Meteorology*, 63,
775 815–822, <https://doi.org/10.1111/j.1600-0889.2011.00540.x>, 2011.

776 Sejr, M. K., Stedmon, C. A., Bendtsen, J., Abermann, J., Juul-Pedersen, T., Mortensen, J., and Rysgaard, S.:
777 Evidence of local and regional freshening of Northeast Greenland coastal waters, *Sci Rep*, 7, 13183,
778 <https://doi.org/10.1038/s41598-017-10610-9>, 2017.

779 Semiletov, I., Makshtas, A., Akasofu, S., and L Andreas, E.: Atmospheric CO₂ balance: The role of Arctic sea ice,
780 *Geophysical Research Letters*, 31, 2003GL017996, <https://doi.org/10.1029/2003GL017996>, 2004.

781 Sievers, Papakyriakou, T., Larsen, S. E., Jammet, M. M., Rysgaard, S., Sejr, M., and Sørensen, L. L.: Estimating
782 surface fluxes using eddy covariance and numerical ogive optimization, *Atmospheric Chemistry and Physics*, 15,
783 2081–2103, <https://doi.org/10.5194/acp-15-2081-2015>, 2015a.

784 Sievers, J., Papakyriakou, T., Larsen, S. E., Jammet, M. M., Rysgaard, S., Sejr, M. K., and Sørensen, L. L.:
785 Estimating surface fluxes using eddy covariance and numerical ogive optimization, *Atmospheric Chemistry and*
786 *Physics*, 15, 2081–2103, <https://doi.org/10.5194/acp-15-2081-2015>, 2015b.

787 Sievers, J., Sørensen, L. L., Papakyriakou, T., Else, B., Sejr, M. K., Haubjerg Søgaard, D., Barber, D., and
788 Rysgaard, S.: Winter observations of CO₂ exchange between sea ice and the atmosphere in a coastal fjord
789 environment, *The Cryosphere*, 9, 1701–1713, <https://doi.org/10.5194/tc-9-1701-2015>, 2015c.

790 Smedman, A., Högström, U., Sahlée, E., and Cecilia, J.: Critical re-evaluation of the bulk transfer coefficient for
791 sensible heat over the ocean during unstable and neutral conditions, *Quart J Royal Meteor Soc*, 133, 227–250,
792 <https://doi.org/10.1002/qj.6>, 2007.

793 Søgaard, D. H., Thomas, D. N., Rysgaard, S., Glud, R. N., Norman, L., Kaartokallio, H., Juul-Pedersen, T., and
794 Geilfus, N.-X.: The relative contributions of biological and abiotic processes to carbon dynamics in subarctic sea
795 ice, *Polar Biol*, 36, 1761–1777, <https://doi.org/10.1007/s00300-013-1396-3>, 2013.

796 Søgaard, D. H., Sorrell, B. K., Sejr, M. K., Andersen, P., Rysgaard, S., Hansen, P. J., Skyttä, A., Lemcke, S., and
797 Lund-Hansen, L. C.: An under-ice bloom of mixotrophic haptophytes in low nutrient and freshwater-influenced
798 Arctic waters, *Sci Rep*, 11, 2915, <https://doi.org/10.1038/s41598-021-82413-y>, 2021.

799 Sørensen, L. L. and Larsen, S. E.: Atmosphere–Surface Fluxes of CO₂ using Spectral Techniques, *Boundary-Layer*
800 *Meteorol*, 136, 59–81, <https://doi.org/10.1007/s10546-010-9499-7>, 2010.

801 Sulpis, O., Lauvset, S. K., and Hagens, M.: Current estimates of K₁* and K₂* appear inconsistent with measured
802 CO₂ system parameters in cold oceanic regions, *Ocean Science*, 16, 847–862, [https://doi.org/10.5194/os-16-847-](https://doi.org/10.5194/os-16-847-2020)
803 2020, 2020.

804 Wanninkhof, R., Asher, W., Ho, D., Sweeney, C., and McGillis, W.: Advances in Quantifying Air-Sea Gas
805 Exchange and Environmental Forcing*, *Annual review of marine science*, 1, 213–44,
806 <https://doi.org/10.1146/annurev.marine.010908.163742>, 2009.

807 Watts, J., Bell, T. G., Anderson, K., Butterworth, B. J., Miller, S., Else, B., and Shutler, J.: Impact of sea ice on air-
808 sea CO₂ exchange – A critical review of polar eddy covariance studies, *Progress in Oceanography*, 201, 102741,
809 <https://doi.org/10.1016/j.pocean.2022.102741>, 2022.

810 Woolf, D. K., Land, P. E., Shutler, J. D., Goddijn-Murphy, L. M., and Donlon, C. J.: On the calculation of air-sea
811 fluxes of CO₂ in the presence of temperature and salinity gradients, *Journal of Geophysical Research: Oceans*, 121,
812 1229–1248, <https://doi.org/10.1002/2015JC011427>, 2016.

813